Application of ASTER Data to Identify Potential Alteration Zones on Microwave Ridge, Northeastern Search Project Area, West-Central British Columbia (part of NTS 093L)

M. Rahimi, Mineral Deposit Research Unit (MDRU), The University of British Columbia, Vancouver, BC, mrahimi@eoas.ubc.ca

J.J. Angen, MDRU, The University of British Columbia, Vancouver, BC

C.J.R. Hart, MDRU, The University of British Columbia, Vancouver, BC

Rahimi, M., Angen, J.J. and Hart, C.J.R. (2018). Application of ASTER data to identify potential alteration zones on Microwave ridge, northeastern Search project area, west-central British Columbia (part of NTS 093L); *in* Geoscience BC Summary of Activities 2017: Minerals and Mining, Geoscience BC, Report 2018-1, p. 7–22.

Introduction

Geoscience BC's Search project (Phase I) area is located between the towns of Smithers and Terrace, British Columbia (BC), and encompasses the western Skeena arch tectonic domain across the Stikine terrane (Figure 1a). This is a highly prospective region that hosts more than 220 metallic mineral occurrences, including abundant vein-type Cu-(Ag-Au) deposits, six of which have historically been mined by hand (e.g., Copper Queen mine, refer to Stock MINFILE 093L 085, BC Geological Survey, 2017). Among the Cu-(Ag-Au) occurrences are numerous examples that are classified as conforming to the volcanic-hosted redbed-copper mineral-deposit model, and others that are assigned to a variety of intrusion-related and subvolcanic mineral-deposit models. There are 54 mineral occurrences that are ambiguously classified as both, despite their mutually exclusive genetic origins.

Distinguishing between these mineral-occurrence types has value for explorers since intrusion-related occurrences are a potential indicator for significant styles of mineralization such as porphyry copper systems, whereas redbed-copper occurrences are not. Methods to potentially discriminate between these two deposit types include gaining a better understanding of their geological setting and identifying the nature of the alteration footprints, which are different for these two mineralization styles. Volcanic-hosted redbed-copper occurrences are typically stratabound and are associated with minimal alteration (Lefebure and Church, 1996), whereas intrusion-related copper veins crosscut stratigraphy, are associated with intrusions and the veins typically have significant sericite-clay– and/or chlorite–alteration zones (Lefebure, 1996) that can be zoned around a central core.

This publication is also available, free of charge, as colour digital files in Adobe Acrobat® PDF format from the Geoscience BC website: http://www.geosciencebc.com/s/SummaryofActivities.asp.

Satellite-acquired infrared spectral data are a valuable source of remotely sensed information that can identify alteration mineralogy that formed from interactions between the hostrock and hot hydrothermal fluids, which may also form metallic mineral deposits. Many alteration minerals (or groups of alteration minerals) have characteristic or diagnostic absorption features that can be remotely detected in infrared spectral data. Advanced Spaceborne Thermal Emission and Reflection Radiometer (ASTER) spectral data, in particular, can be utilized to remotely map the distribution of specific minerals that form different types of alteration potentially related to mineralizing processes. Such remote-sensing technologies have been widely and successfully used for lithological and alteration-mineral mapping as a contribution to mineral exploration efforts (Watts and Harris, 2005; Azizi et al., 2010; Rajendran et al., 2012; Van Ruitenbeek et al., 2012).

Microwave ridge is an informal name given to a northwest-trending ridge in the central portion of the Skeena arch, approximately 15 km southwest of Hudson Bay Mountain, west of the town of Smithers (Figure 1a). This area hosts three ambiguously assigned Cu-(Ag-Au) occurrences and was chosen to test the effectiveness of alteration mapping using ASTER data in distinguishing between intrusion-related and volcanic-hosted redbed-copper types of mineral occurrences. Microwave ridge is an ideal location due to the relatively simple geology of this area, such that variations in spectral responses are likely the product of hydrothermal alteration, and not simply caused by the underlying lithology.

Geological Setting

Regional Geology

The Skeena arch is an east-northeast-trending geomorphological belt that transects the Stikine terrane in central BC. It is underlain by Mississippian through Neogene rocks that record the transition from island-arc magmatism and re-

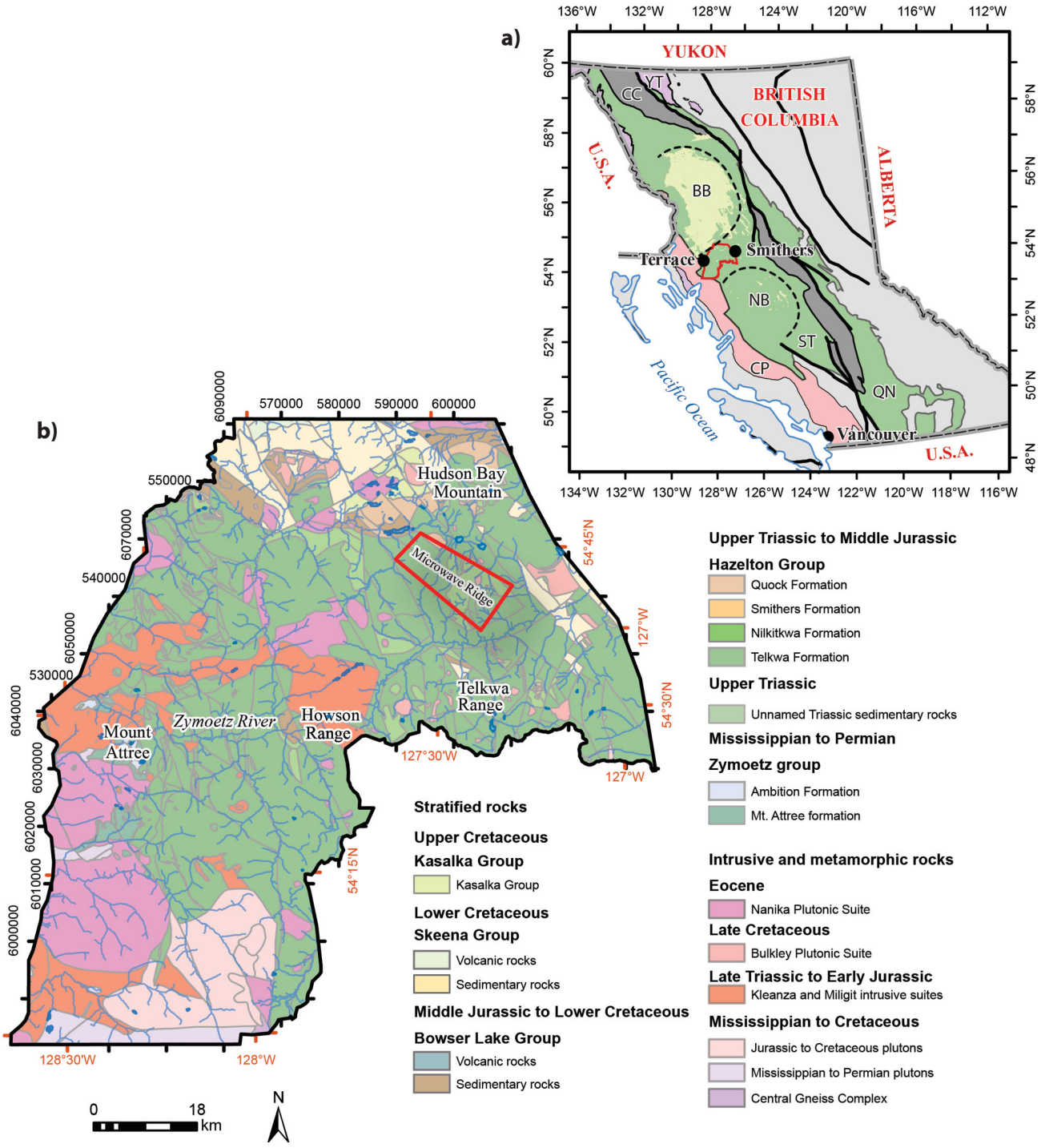

Figure 1. Search project in west-central British Columbia: **a)** location of the area of interest within the context of selected terranes and tectonic elements in British Columbia, including the Cache Creek (CC), Quesnel (QN), Stikine (ST) and Yukon-Tanana (YT) terranes, Coast Plutonic Complex (CP), Bowser Basin (BB) and Nechako Basin (NB)—the Skeena arch corresponds to the region between the Bowser and Nechako basins (terranes modified after Colpron and Nelson, 2011; strata deposited in the Bowser and Nechako basins modified after Cui et al., 2015); **b)** simplified geology of the area of interest, with the outline of the Microwave ridge study area in red (distribution of rock units modified after Cui et al., 2015). Place name with the generic in lower case is unofficial.

lated sedimentation of the Stikine terrane to post-accretionary continental-margin–arc magmatism and sedimentation of the overlap assemblages. The oldest rocks are primitive-arc volcanic rocks of the Mississippian to Permian Mt. Attree formation, which form isolated exposures in the western Search project area (Figure 1b; Nelson et al., 2008). They are overlain by Permian limestone of the Ambition Formation and an unnamed Middle Triassic unit of thin-bedded chert and argillite (Nelson et al., 2006). Mississippian to Permian intrusions in the southwestern corner of the Search project area occur with younger intrusions and metamorphic rocks that make up the Coast Plutonic Complex (Figure 1a).

The most widely exposed rock unit is the uppermost Upper Triassic to Lower Jurassic Telkwa Formation of the Hazelton Group. At the latitude of the Skeena arch, the Telkwa Formation has been subdivided into the western Howson subaerial facies, the central Babine shelf facies and the eastern Kotsine submarine facies (Tipper and Richards, 1976a). The Search project area is mostly within the Howson facies, named after the Howson Range (Figure 1b). The transition easterly from the Howson to the Babine facies is marked by increasing proportions of sedimentary rocks. The Kleanza intrusive suite is the plutonic equivalent of the Telkwa Formation (Nelson, 2017). Slightly older Late Triassic intrusive rocks in the Howson Range are herein called the Miligit intrusive suite (Figure 1). The proportion of sedimentary rocks also increases upsection within the Hazelton Group. The Telkwa Formation is conformably and locally gradationally overlain by mixed sedimentary and volcanic strata of the Nilkitkwa Formation (Pliensbachian to Toarcian; Tipper and Richards, 1976a). The Nilkitkwa Formation includes the Red Tuff Member: a sequence of well-bedded, brick red, crystal-lithic Toarcian tuff, with minor basalt and rhyolite that are (nearly) indistinguishable from the red tuffs in the upper Telkwa Formation (Tipper and Richards, 1976a). The Nilkitkwa Formation is overlain by tuffaceous sandstone of the Smithers Formation (Toarcian to Bathonian) and tuffaceous mudstone of the Quock Formation (Bajocian to Callovian; Gagnon et al., 2012).

The Hazelton Group is gradationally overlain by siliciclastic rocks of the Bowser Lake Group (Figure 1b). The uppermost distinguishable tuff bed within a sequence of deep marine sedimentary rocks marks the boundary between these two groups along the southern margin of the Bowser Basin (Evenchick et al., 2010). Middle Jurassic to Lower Cretaceous sedimentary rocks of the Bowser Lake Group are rare across most of the Skeena arch, which supports it being interpreted as a topographic highland that formed the southern boundary of the Bowser Basin and the northern boundary of the Nechako Basin at that time (Tipper and Richards, 1976a). In the central Skeena arch, the Bowser Lake Group is absent and Lower to Upper Cretaceous sedimentary and volcanic rocks of the Skeena Group unconformably overlie the Telkwa Formation (Figure 1b; Palsgrove and Bustin, 1991). The Upper Cretaceous Kasalka Group volcanic rocks locally overlie the Skeena Group (Figure 1b).

The Late Cretaceous Bulkley and Eocene Nanika plutonic suites are widespread across the Skeena arch (Figure 1b). They typically occur as small stocks, dikes and sills of diorite to monzogranite. The majority of mineralization within the Skeena arch is associated with these Late Cretaceous and Eocene intrusions (MacIntyre, 2006).

Microwave Ridge Geology

Microwave ridge is underlain by a series of moderately northeast- to southeast-dipping homoclinal panels of Telkwa Formation volcanic rocks that are separated by northwest-trending faults with minimal displacement (Figure 2). The Telkwa Formation in this area includes a lower unit of andesitic lapilli tuff, aphyric basalt and rhyolite lenses; a middle tuffaceous sedimentary unit; and an upper unit of quartz-bearing dacitic tuff. The stratified rocks are cut by isolated intrusions that are interpreted as belonging to the Bulkley Plutonic Suite (Figure 2).

Lower Telkwa Formation Andesitic Tuff Unit

The lower Telkwa Formation on Microwave ridge includes fine-grained basalt flows, andesitic to dacitic lapilli tuff and ash tuff, rhyolite lenses and minor interbedded sedimentary rocks. Basalt flows are typically aphyric, fine grained and dark grey, with purple and maroon pumiceous flow-top breccias (Figure 3a). They locally contain chlorite- or calcite-filled amygdules and well-developed Liesegang rings. Zeolite- and epidote-cemented flow-top breccias were reported by MacIntyre et al. (1989b). Basalt flows are 2–10 m thick and are not laterally continuous. They are interpreted to fill paleotopographic depressions and/or scoured lava-flow channels. Lapilli-tuff beds are maroon to brick red, with fragments of plagioclase-phyric andesite, cream-coloured rhyolite and dark grey basalt, as well as up to 15% plagioclase-crystal fragments. One lapilli-tuff bed at the top of this sequence includes 3% quartz-crystal fragments. Individual tuff beds vary from 10 cm to 5 m in thickness and are laterally continuous.

Middle Telkwa Formation Sedimentary Unit

A lens of epiclastic conglomerate, siltstone, calcareous tuff and limestone bisects Microwave ridge and overlies the quartz-bearing lapilli tuff described above (Figure 2). Conglomerate beds contain well-rounded cobbles to boulders of volcanic rock units similar to the underlying lower Telkwa Formation within a coarse sand matrix (Figure 3b). Carbonate-rich sandstone and tuff beds weather recessively (Figure 3b). Fine- to coarse-grained epiclastic sandstone occurs in planar beds 5–10 cm thick, some of which fine up-

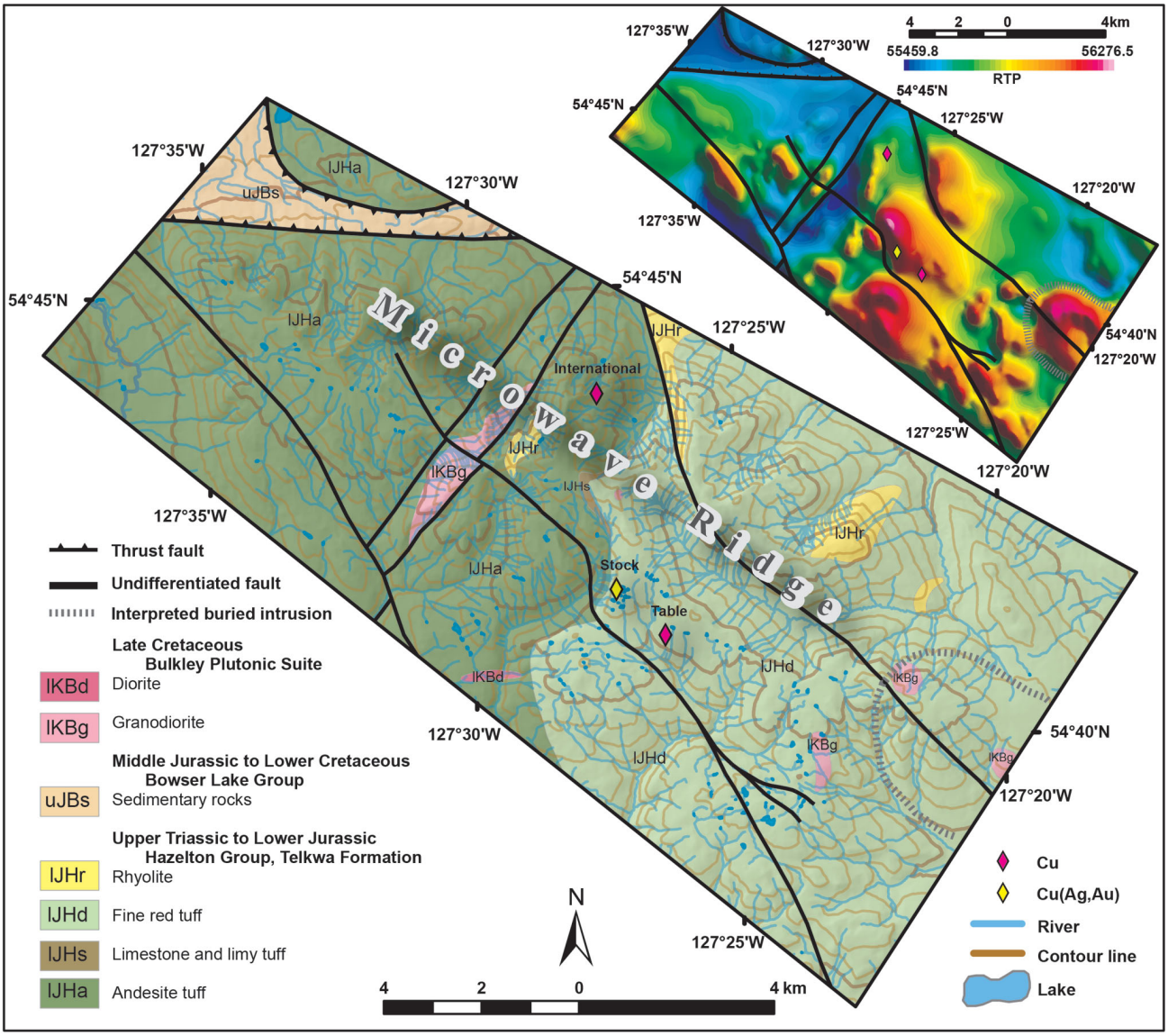

Figure 2. New geological interpretation for Microwave ridge, west-central British Columbia, integrated from previous geological mapping (Tipper and Richards, 1976b; MacIntyre et al., 1989a), aerial photographs, new aeromagnetic data and ground truthing. Inset is reduced-to-pole aeromagnetic data for the Microwave ridge area (modified after Precision GeoSurveys Inc., 2016).

ward into maroon mudstone. MacIntyre et al. (1989b) reported pure limestone as a component of this sedimentary sequence.

MacIntyre et al. (1989b) interpreted this lens as part of the Nilkitkwa Formation. Desjardins et al. (1990) interpreted a similar fossiliferous sedimentary sequence in the Thautil River map area to the south as a component of the Telkwa Formation. Stanley and McRoberts (1993) studied a Sinemurian reef in the Thautil River map area, which they assigned to the Nilkitkwa Formation, yet also acknowledged that other workers consider it to be part of the Telkwa Formation. New, preliminary U-Pb zircon analyses of samples bracketing the sedimentary sequence on Microwave ridge yield overlapping ages of 197.5 ±2.6 Ma and 201.5 ±1.5 Ma. The Nilkitkwa Formation, as originally described, is dominantly black mudstone, with abundant Pliensbachian fossils in the base of the unit as well as restricted Toarcian volcanic rocks (Tipper and Richards, 1976a). These shallow-marine sedimentary rocks are interbedded with Hettangian to Sinemurian volcanic rocks, which indicates that they are not part of the Nilkitkwa Formation but are rather a sedimentary inlier of the Telkwa Formation. Tipper and Richards (1976a) reported isolated marine sedimentary rocks, including limestone interbedded with subaerial volcanic rocks, at the transition zone between the Howson and Babine facies of the Telkwa Formation.

Upper Telkwa Formation Dacitic Tuff Unit

The upper Telkwa Formation is dominated by brick red dacitic lapilli, crystal and ash tuff, with minor rhyolite,

sandstone and siltstone. Dacitic tuff beds vary from 5 cm to 5 m in thickness and are normally graded. Lapilli-tuff components contain maroon and purple, aphanitic to sparsely plagioclase-phyric lapilli, rare beige rhyolitic lapilli, up to 3% quartz-crystal fragments and 5–10% feldspar-crystal fragments in fine red-ash groundmass. Some beds contain accretionary lapilli (Figure 3c). This section includes interbedded sandstone and siltstone. The upper contact of the Telkwa Formation is not exposed in this area.

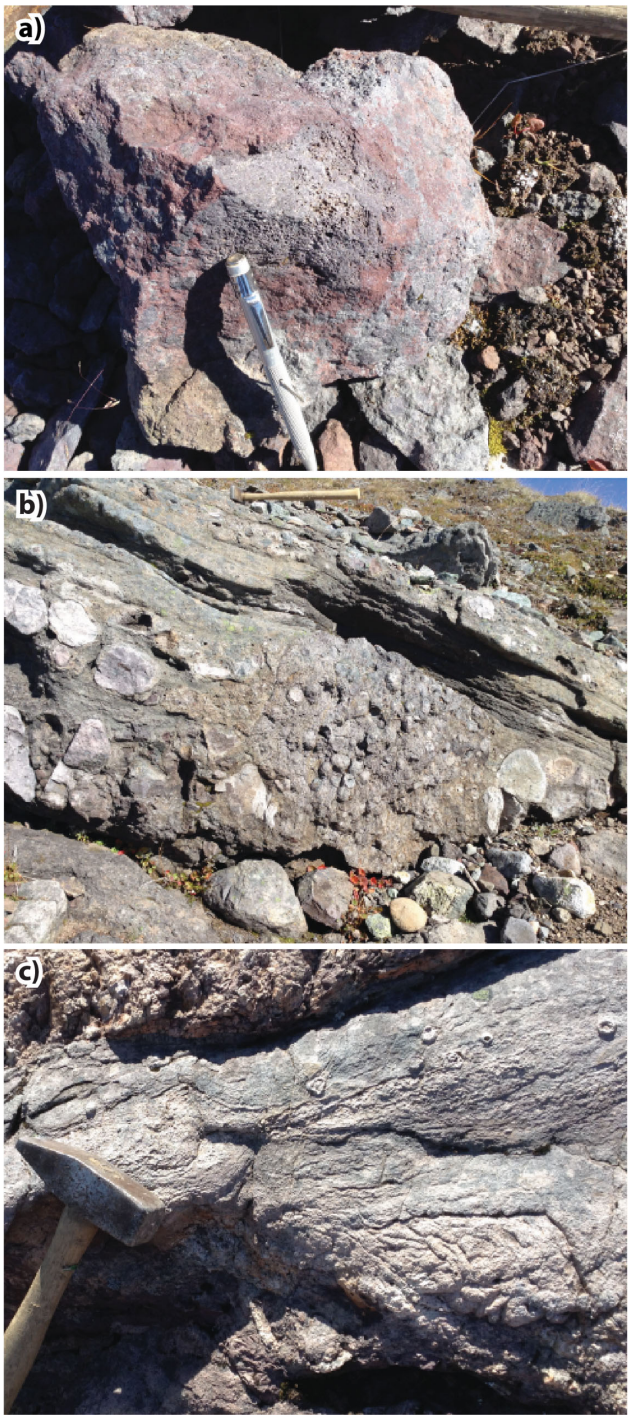

Figure 3. Characteristic rock units of the Telkwa Formation on Microwave ridge, west-central British Columbia: **a)** pumiceous breccia in Telkwa Formation basalt; **b)** Telkwa sedimentary unit, with conglomerate and recessively weathering limy epiclastic sandstone; **c)** Telkwa Formation red dacite tuff, with accretionary lapilli.

Telkwa Formation Rhyolite

Rhyolite lenses up to 2 km wide and 1 km thick occur within the lower and upper volcanic units on Microwave ridge (MacIntyre et al., 1989b). They include flow-banded and spherulitic flow domes, which locally intrude older volcanic rocks, but also occur as concordant lapilli-tuff accumulations. These centres of rhyolite contain trace to 2% pyrite and typically lack quartz phenocrysts. Some fine-grained felsic exposures were previously interpreted as Cretaceous or Eocene felsite intrusions (Tipper and Richards, 1976b; MacIntyre et al., 1989a). The presence of rhyolite lapilli fragments within red-tuff beds indicates that at least some of the rhyolite belongs to the Telkwa Formation. Where Telkwa Formation rhyolite flow domes and breccias occur elsewhere in the Search project area, they have low magnetic susceptibilities (average of 0.2×10^{-3} SI based on data collected by the authors) in contrast to the much younger Bulkley and Nanika felsic intrusive suites (see below). Felsic intrusions mapped as 'felsite' on Microwave ridge by Tipper and Richards (1976b) and MacIntyre et al. (1989a) lack corresponding high aeromagnetic anomalies and are therefore tentatively interpreted as Telkwa Formation rhyolite and not younger intrusions.

Bowser Lake Group

In the valley north of Microwave ridge, there is a domain of low magnetic response (Figure 2 inset). This corresponds to an area that is interpreted to be underlain by Bowser Lake Group sedimentary rocks (Tipper and Richards, 1976b). Where the Bowser Lake Group is exposed farther west, it includes well-bedded sandstone, siltstone and minor granule conglomerate with Callovian shallow-marine fossils (Tipper and Richards, 1976a). This domain is in fault contact with the Telkwa Formation to the north and south (Figure 2).

Bulkley (or Nanika) Plutonic Suite

Isolated exposures of quartz-feldspar porphyry and diorite on Microwave ridge were assigned previously to the Bulkley (or Nanika) Plutonic Suite (Tipper and Richards, 1976b; MacIntyre et al., 1989a). The Bulkley Plutonic Suite in the Search project area typically consists of quartz-phyric diorite to granodiorite, and the Nanika Plutonic Suite intrusions are typically porphyritic monzogranite to diorite. Both plutonic suites contain magnetite that results in typically high average magnetic susceptibilities (combined average of 7.7×10^{-3} SI, based on data collected by the authors). As noted by Angen et al. (2017), these units typically correspond to regions of high aeromagnetic response. Both units are also associated with significant mineralization in the Skeena arch (MacIntyre, 2006).

Two previously mapped exposures of quartz-feldspar–phyric granodiorite (Tipper and Richards, 1976b; MacIntyre et al., 1989a) at the southeastern end of Microwave ridge are within a ~3 km long ovoid-shaped aeromagnetic high that likely indicates a buried magnetite-bearing intrusion (Figure 2). A pronounced northeast-trending aeromagnetic high bisects Microwave ridge and corresponds to two parallel faults that were mapped by Tipper and Richards (1976b; Figure 2 inset). This aeromagnetic high corresponds to resistant, light grey, massive rocks that are exposed between well-bedded maroon volcanic rocks to the northwest and southeast, as observed in aerial photographs. These light grey rocks are interpreted as a probable magnetite-bearing granodiorite dike. All of the magnetic intrusive rocks that are exposed on Microwave ridge are tentatively assigned to the Bulkley Plutonic Suite.

Structure of Microwave Ridge

Numerous northwest-trending faults, identifiable from minor linear topographic depressions, are visible in aerial photos. Most faults are minor and only a few hundred metres long with no significant impact on the geology. A few are more continuous and separate structural domains that have internally consistent bedding orientations (Figure 2).

A thrust fault juxtaposes the Telkwa Formation on Microwave ridge on top of sedimentary rocks of the Bowser Lake Group (Tipper and Richards, 1976b). A top-to-the-north displacement component is inferred, since the footwall exposures are some of the southernmost exposures of Bowser Basin rocks (Tipper and Richards, 1976a). The age of the thrust is uncertain but must be younger than Callovian, based on the age of the rocks in the footwall. Fault movement is likely coeval with the Early Cretaceous or younger northeast-trending folds and northwest-vergent thrust faults that are documented elsewhere in the Skeena arch (Angen et al., 2017).

ASTER Spectral Data

The Advanced Spaceborne Thermal Emission and Reflection Radiometer (Jet Propulsion Laboratory, 2017) is a multispectral imager. The imager was launched on the panel of the National Aeronautics and Space Administration (NASA) Terra spacecraft in December 1999 (Kalinowski and Oliver, 2004). The most important feature of ASTER images, in comparison with other multispectral images, is that ASTER covers a wide spectral zone with 14 bands from the visible to the thermal infrared. The ASTER images provide high spatial, spectral and radiometric resolution compared to other images used in the earth sciences, such as Landsat 7 ETM+ and Landsat 8 (OLI). The wavelength range of 2–2.5 micrometres (µm) is the most suitable part of the spectrum for identifying hydroxyl-bearing minerals, carbonates and iron oxides, which have a significant absorption feature in this range; all of these mineral groups include important products of hydrothermal alteration. This wavelength range is mostly covered by a single band (band 7) in Landsat 7 ETM+ and Landsat 8, whereas it is divided into five bands in ASTER data; therefore, ASTER data allows for better distinction between these minerals of interest. Data acquired using ASTER include visible- and near-infrared (VNIR) radiation recorded in three spectral bands (0.52–0.86 µm, 15 m spatial resolution); shortwave-infrared (SWIR) radiation, in six spectral bands (1.6–2.43 µm, 30 m spatial resolution); and thermal-infrared (TIR) radiation, in five bands (8.12–11.65 µm, 90 m resolution). Each ASTER scene covers an area of 60 by 60 km. New AST L1T images in hierarchical data format are freely downloadable from NASA or the United States Geological Survey (USGS) ASTER archive (United States Geological Survey, 2017).

Pre-Processing

Geometric and radiometric corrections have been carried out by NASA/USGS on the original AST L1A images to produce AST L1T. These calibrations and corrections include radiometric calibration, geometric processing, and corrections for the SWIR crosstalk. Also, scene registration corrections for SWIR and TIR are applied to SWIR for parallax errors as a result of spatial locations of the bands. To get the best images of the area of interest by converting radiance to reflectance on the ground, an atmospheric correction algorithm was applied on the NASA datasets. In this project, the internal average relative reflectance algorithm was used to calibrate the image.

A variety of masking techniques were applied in order to reduce image spectral variability (Mather, 1999) to that which is related to the exposed bedrock surface. The normalized difference vegetation index was used to mask the vegetation. Dark-object subtractions were applied to the images to mask the dark pixels in shadows, based on their digital number (DN) values. For ice and snow, target DN values were determined using false-colour composites. This method helps to keep the areas that have light and scattered snow coverage in the datasets. Since scenes with less than 10% cloud coverage were initially obtained, the area with cloud coverage was very limited; however, these areas were also removed from the cloud mask final result.

Processing

To obtain the most reliable results, three ASTER scenes with considerable overlap were processed (Table 1). The methods of band ratio (BR), relative absorption band depth (RBD), least squares fit (LS-Fit), linear spectral unmixing (LSU) and matched filtering (MF) were applied individually in conjunction with each pre-processed scene to detect specific alteration minerals, including epidote, chlorite, calcite, muscovite, kaolinite and alunite, as well as iron-ox-

Table 1. ASTER scenes utilized to identify potential alteration on Microwave ridge in west-central British Columbia.

Granule ID	Centre Latitude	Centre Longitude	Acquisition date	Acquisition time	Sun azimuth
AST_L1T_00308142001194937_20150501182409_113892	54°47'18.24"N	127°06'57.96"W	14/08/2001	49:37.7	164.139311
AST_L1T_00302172001200556_20150414212851_118220	54°58'00.84"N	127°40'42.96"W	17/02/2001	05:56.4	169.94084
AST_L1T_00309042006194746_20150516010940_107577	54°40'38.64"N	127°53'05.28"W	04/09/2006	47:46.3	165.567025

ide and ferric iron-bearing minerals. A summary of the steps of ASTER-image processing from data to output is shown on Figure 4.

Band Ratio (BR) Method

Band ratio is one of the basic methods used for image processing; each pixel in the image has a specific DN for each band. In the BR technique, a ratio of two DN values is calculated for each pixel to generate a new set of DN values. This method reduces the effect of illumination variability, based on the interpretation that radiance across the entire spectrum will be proportional to illumination: a region in direct sunlight will have much greater radiance than a region in shadow but the ratio of any given two bands should be similar if the surface material is the same (Husdal, 1999). The DN value of a single band is highly dependent on illumination, whereas pixels representing the same material will return similar ratios, significantly reducing the effect of topography (Sabins, 1997). The BR technique applied to ASTER imagery has been widely used in alteration mapping (Hewson et. al., 2001; Bierwirth, 2002; Rowan et. al., 2003; Mars and Rowan, 2006; Palomera, 2015; Commonwealth Scientific and Industrial Research Organisation, 2017).

Relative Absorption Band Depth (RBD) Method

The RBD technique is used to represent the spectral contrast of a specific absorption feature and has been broadly used for geology and alteration mapping (Rowen and Mars, 2003). The method works based on the maximum and minimum values around an absorption feature. As with the BR technique, this method reduces the effect of topography (Crowley et al., 1989). In this technique, first the appropriate absorption feature is selected for a given material of interest. Then bands near the shoulder and the minimum of the absorption feature are selected, and the algorithm is applied to the data (Van der Meer et. al., 2008). The sum of the reflectance values at the shoulder of the targeted spectral band(s) is divided by the sum of reflectance values at the minimum (Crowley et al., 1989; Ramachandran et al., 2010). The result includes a set of pixels that have a range of DN values related to the potential presence of a certain mineral; therefore to map the most likely areas, mask-threshold values should be applied to the results of RBD analysis.

Least Squares Fitting (LS-Fit) Method

The LS-Fitting method is based on band simulation and assumes that the bands used as input values are performing as the variables of a linear expression. In this method, a predicted band that includes the spectral characteristics of target minerals is selected. The algorithm calculates the output value from this band (Asadi Haroni and Lavafan, 2007). Then a set of bands are selected to put in the model as predictor bands. By applying correlation coefficients on predictor bands, a model prediction-band value is calculated that can be compared with the predicted-band value.

The results of the method include a model prediction band and a residual band. The residual band actually represents the difference between the prediction band and the predicted band in the form of an image for the target material. In the hypothetical case where a pixel represents exactly the material of interest, the model prediction-band value, based on predictor bands, will be equal to the real predicted-band value and the residual will be zero. Since the pixels are not pure, they may have a lower response than the expected amount for the target material in the predicted band. This method is a knowledge-based method and the predicted and predictor bands are selected based on expert knowledge of mineralogical assemblages expected to occur in the area of interest.

Linear Spectral Unmixing (LSU) Method

The LSU method is a supervised classification technique that defines relative abundances of minerals using their spectral characteristics. Pixels in the ASTER images are not pure and the value of each pixel is based on a mixture of the spectral characteristics of different minerals. In this approach, the unmixing coefficients are detected by minimizing the sum of the squares of the errors (Shimabukuro and Smith, 1991). Depending on the complexity of the scene, as well as the number and the wavelengths of the bands used, different numbers of end members contribute to the model (Tseng, 2000).

The results of LSU provide a series of single-band images for each target mineral. The reference spectra for this study

were selected from the USGS spectral library, based on the geological knowledge of the area of interest, and include spectra of kaolinite, alunite, muscovite, calcite, epidote, chlorite, jarosite, hematite, goethite and limonite. The USGS spectra were resampled to the number of ASTER bands selected for this analysis (Figure 5). Selected pixel spectra taken from each ASTER granule are processed using the new spectral library.

Matched Filtering (MF) Method

The MF method is also a supervised classification technique. The model achieves a partial unmixing of spectra; therefore it is not essential to find the spectra of all end members in the image. The method filters the image to define the best matches of the selected spectra for the target minerals by detecting the abundance of defined end members. In this technique, the known end member is processed and the result of the responses is maximized, then the unknown composite of the dataset is predicted using the results from the processing of the known end member. The method increases the possibility of obtaining an accurate analysis. The result of this process includes a set of images, each corresponding to a specific mineral. The brightest pixels in this image represent the highest probability of the presence of a specific mineral in the target spatial dataset (Boardman et al., 1995).

Results and Discussion

A natural-colour composite of ASTER bands 2, 3 and 1 (RGB) for the area of interest emphasizes the contrast between bedrock exposure and vegetation coverage (Fig-

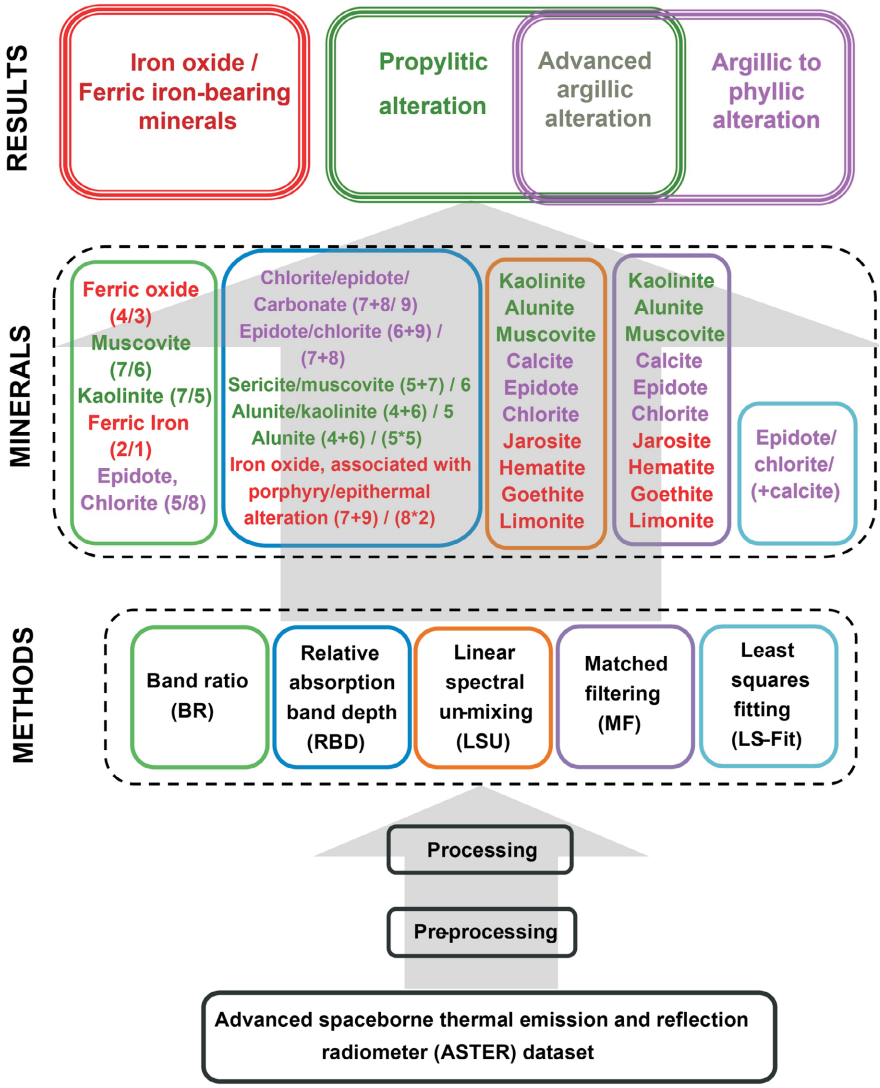

Figure 4. Processing workflow for ASTER data, showing the methods used to generate intermediate maps for specified minerals or groups of minerals. The numbers in the mineral row indicate the ASTER bands used in calculations. The coloured text in the mineral row indicates the intermediate maps that were used to generate the corresponding final output maps in the results row.

ure 6a). The results of BR and RBD are raster images with multiple DN values. The DN values are acquired by applying the proper thresholds and reflecting the proportional amounts of the targeted minerals interpreted to be within a given pixel. Clustered high DN values are considered to be probable alteration zones. These intermediate maps were merged with other results to generate the maps discussed below.

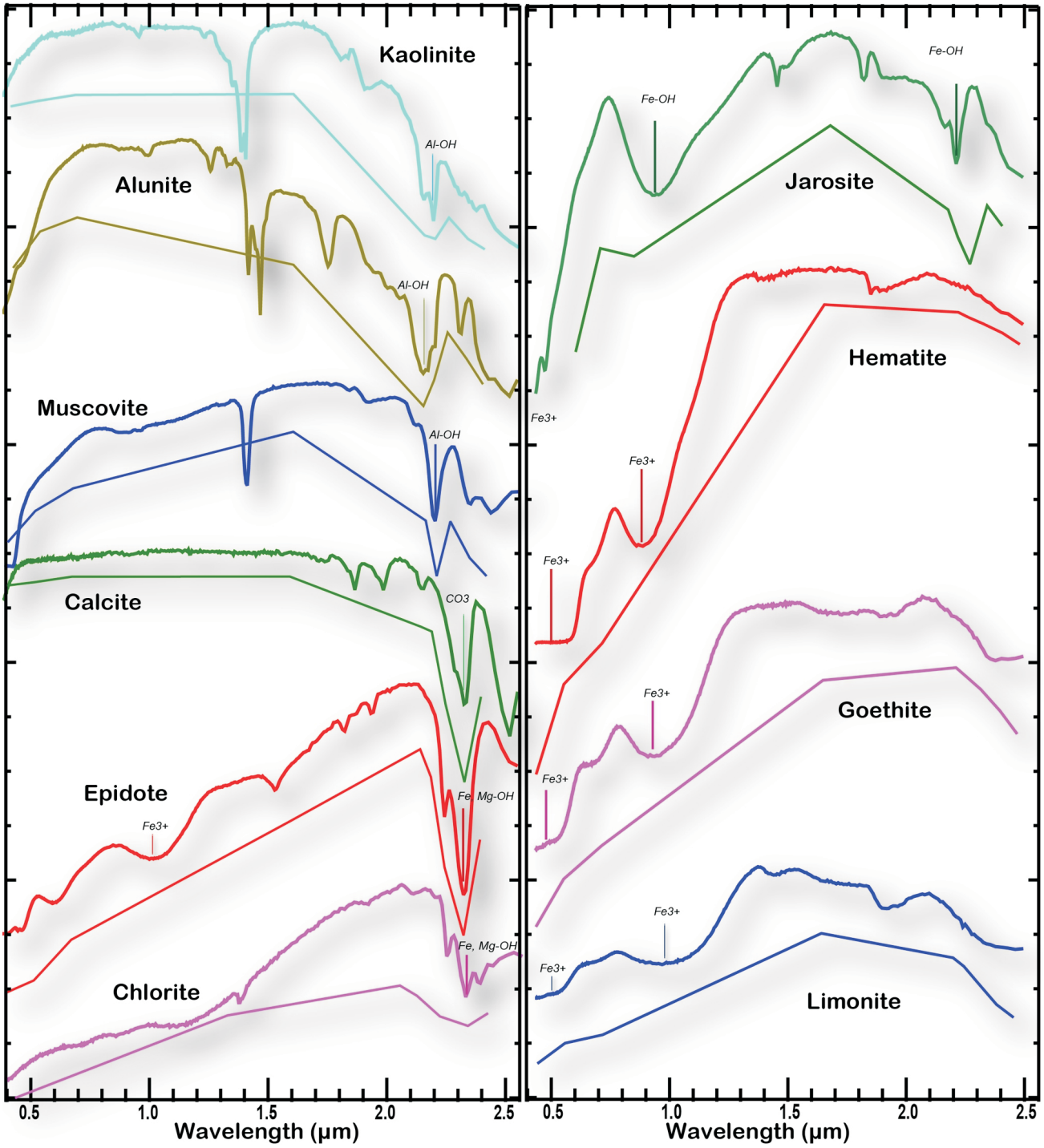

Figure 5. Comparison between laboratory spectra of kaolinite, alunite, muscovite, calcite, epidote, chlorite, jarosite, hematite, goethite and limonite, and their equivalents, resampled to ASTER bands. The upper line for each mineral is the laboratory spectra and the lower line is the resampled equivalent. Calcite has a prominent 2.33 μm CO_3 absorption feature; limonite has a broad 0.66–1.165 μm Fe^{3+} absorption feature; kaolinite, muscovite and alunite have Al-OH absorption features at 2.165, 2.20 and 2.20 μm, respectively; and epidote and chlorite have an Fe-Mg-OH absorption feature at 2.32 μm (modified after Clark et al., 1993; Ramachandran et al., 2010; Beiranvand Pour and Hashim, 2014).

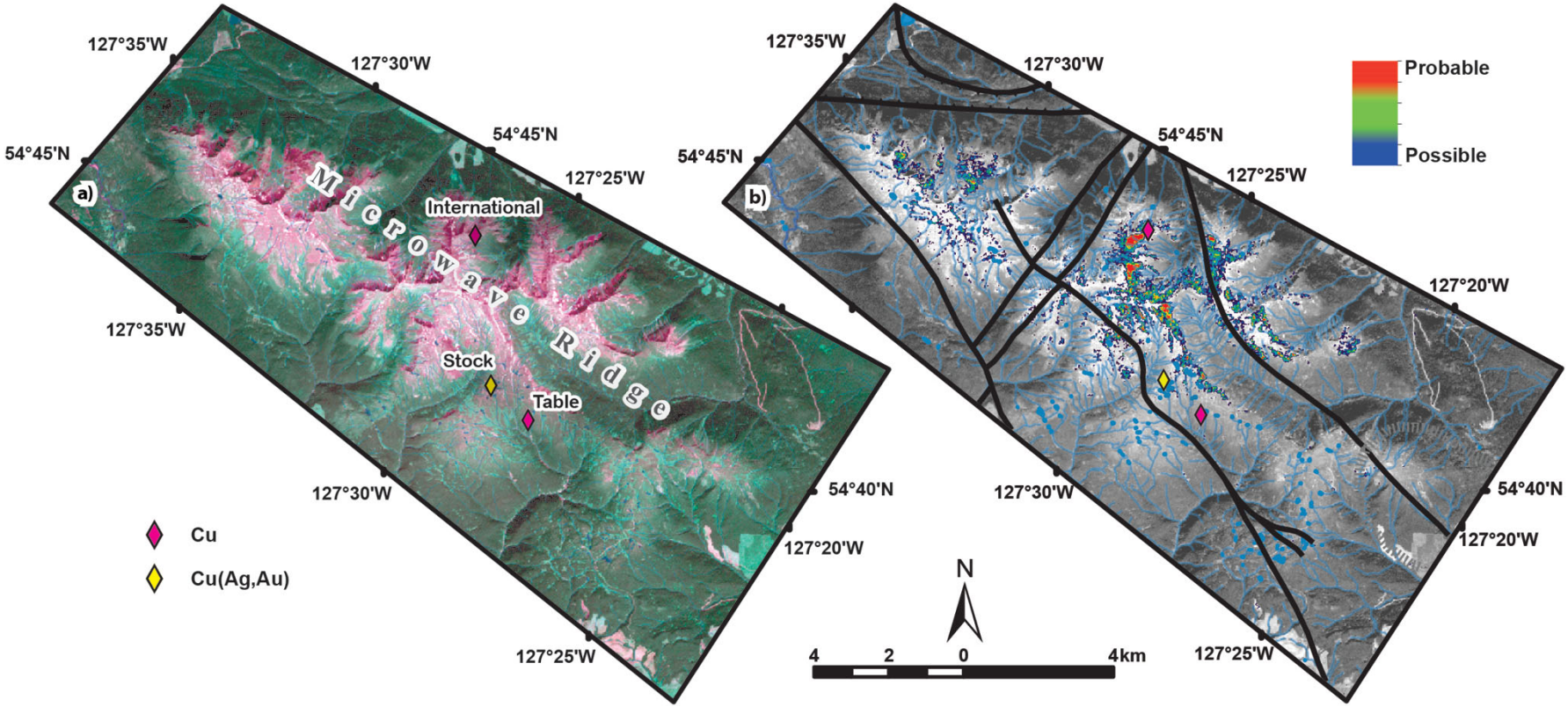

Figure 6. Results of processing ASTER data from Microwave ridge in west-central British Columbia for epidote and chlorite (±calcite): **a)** ASTER natural-colour composite using bands 2, 3 and 1 (RGB) emphasizes the contrast between bedrock and vegetation; **b)** pseudo-colour image generated by the LS-Fitting method displays the results for epidote, chlorite and possibly calcite minerals; red represents the highest concentration, whereas dark blue represents the lowest concentration for pixels where these minerals were detected.

The intensity of absorption at band 8 is presented in Figure 6b. This absorption feature is characteristic of Mg-OH–bearing minerals such as epidote and chlorite, which are a significant component of propylitic alteration. Band 8 is also sensitive to carbonate minerals, which are also present in propylitic alteration zones. A combination of BR, RBD and LS-Fit processing has been applied to detect these minerals. There is a low-intensity response across much of the exposed bedrock on Microwave ridge that likely reflects background chlorite, epidote and carbonate, which occur in small amounts throughout the Telkwa Formation (Figure 6b). By filtering out everything except the highly anomalous responses, three distinct potential alteration zones and a few minor outliers stand out (Figure 7a), the southernmost of these three possible alteration zones is centred on a region previously-mapped as granodiorite (Tipper and Richards, 1976b). It is possible that the two, more northerly alteration zones of anomalous response correspond to either unmapped or unexposed granodiorite, with corresponding hydrothermal alteration zones.

Absorption at 2.22–2.24 μm (band 6) is characteristic of Al-OH–bearing minerals including, kaolinite, alunite and sericite (muscovite), which may reflect argillic (kaolinite), advanced argillic- (alunite) or phyllic- (sericite) alteration mineral assemblages. A combination of BR, RBD, LSU and MF processing has been applied to detect these minerals. Regions where ASTER data indicate potentially anomalous concentrations of these minerals are presented along with the Mg-OH data in Figure 7a. This processing has identified many widely distributed zones of potential kaolinite, alunite and/or sericite. Clay minerals produced from the weathering of feldspar typically contain Al-OH, therefore interpretation of the Al-OH results must be done with caution since these identified zones may simply reflect weathering. However, it is notable that the three potential propylitic-alteration zones identified above are apparently flanked by zones of Al-OH–bearing minerals.

A combination of BR, RBD, LSU and MF techniques was applied to detect iron-oxide and ferric iron-bearing minerals, such as hematite, goethite and jarosite (Figure 8a–d). There appears to be a correlation between interpreted iron-oxide and ferric iron-bearing minerals and northwest-trending faults, which may indicate structurally controlled hydrothermal alteration. This is particularly evident around the fault closest to the Table and Stock prospects (Figure 8a). Structurally controlled ferric iron-oxide alteration could be the product of low-temperature hydrothermal fluids associated with volcanic-hosted redbed-copper mineralization (Lefebure and Ray, 1998). The three overlapping zones identified in Figure 7a also correspond to possible Fe-oxide and ferric iron-bearing alteration zones (Figure 7b).

Understanding the distribution of rock units is critical to adequately interpreting the results of ASTER processing. The unaltered rock units on Microwave ridge are not likely to yield significantly different responses for any of the selected processing methods. Therefore, the identified zones are interpreted to reflect potential zones of alteration rather than simply differences in rock type.

The results of ASTER processing suggest the presence of three potential zones of overlapping Mg-OH–bearing ±carbonate minerals, Al-OH–bearing minerals and iron oxides. One of these overlapping zones corresponds to a location previously mapped as Bulkley Plutonic Suite granodiorite. It is possible that the other two correspond to alteration related to Bulkley granodiorite that is either unrecognized or blind. The International (MINFILE 093L 086) occurrence is located along the margin of the northernmost alteration zone. The showing consists of minor disseminated chalcopyrite and fractures lined with malachite within amygdaloidal basalt; on its own, this minor copper showing may be of little interest (Robertson, 1917). The hydrothermal fluid responsible for these overlapping zones of alteration may be related to the Bulkley Plutonic Suite intrusion(s) with potential for other, more significant styles of mineralization nearby.

The noted lack of alteration identified through ASTER processing in the immediate vicinity of the Stock (MINFILE 093L 085) and Table (MINFILE 093L 084) occurrences, combined with iron-oxide–dominated alteration along associated northwest-trending minor faults, suggest that these occurrences formed from relatively low-temperature hydrothermal fluids. This is likely consistent with either a volcanic-hosted redbed-copper style of mineralization, or potentially a cool and distal expression of an intrusion-related hydrothermal fluid, as opposed to a proximal higher temperature intrusion-related hydrothermal fluid. Either way, these occurrences are poorer indicators of nearby intrusion-related mineralization.

Conclusion

The Microwave ridge area is a dominantly east-dipping structural panel that exposes a section through the Telkwa Formation that is cut by small, Late Cretaceous (or Eocene) intrusions. A calcareous epiclastic sedimentary horizon that had previously been assigned to the Nilkitkwa Formation is reinterpreted as a local sedimentary inlier within the dominantly volcanic Telkwa Formation. Rhyolite lenses within the sequence are interpreted as isolated Telkwa Formation rhyolitic eruptive centres. They are distinguished from porphyritic Late Cretaceous or Eocene intrusions, in part, by their lack of aeromagnetic response.

Processing of ASTER data has identified three potential zones of overlapping kaolinite+alunite+sericite, epidote+

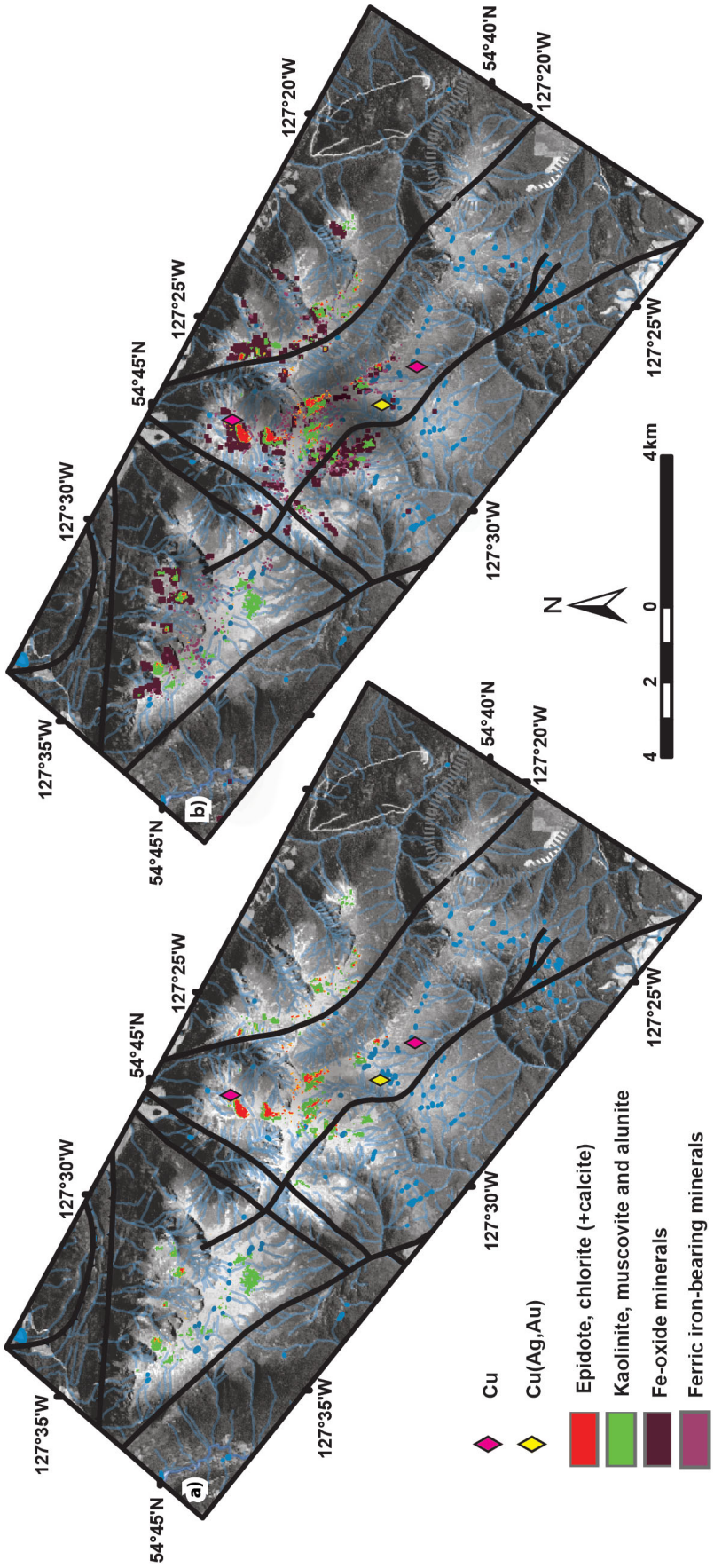

Figure 7. Zones of strongest response for the mineral groupings investigated at Microwave ridge in west-central British Columbia: **a)** the highest responses for epidote and chlorite (±calcite) are plotted in red, along with kaolinite, muscovite and alunite in green; **b)** the highest responses for Fe-oxide zones are plotted in purple, along with ferric iron-bearing zones (including ferric oxides) in pink, overlain on the responses plotted in Figure 7a.

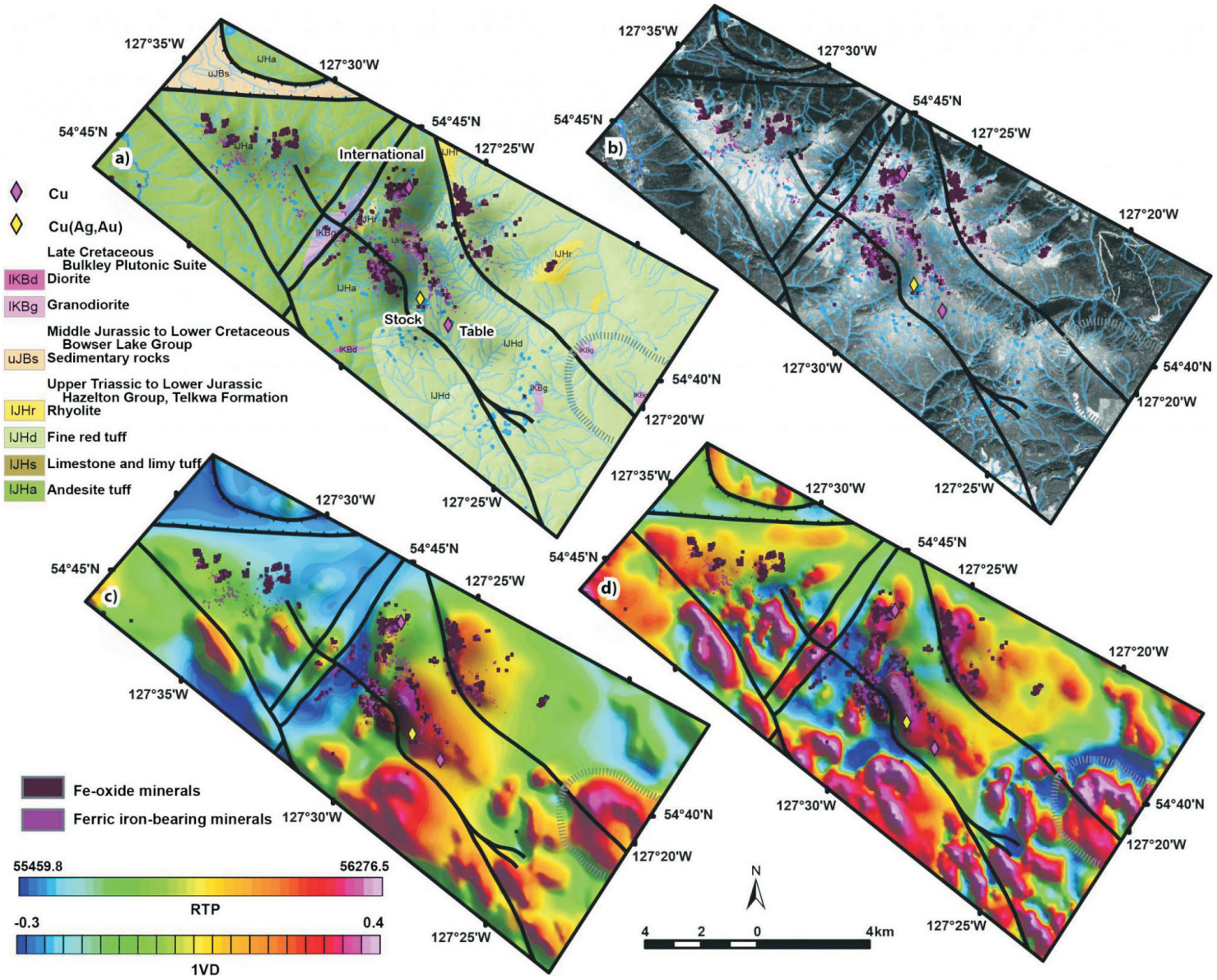

Figure 8: Zones of Fe-oxide (purple) and ferric iron-bearing (pink) minerals in the Microwave ridge area, west-central British Columbia, that were detected through BD, RBD, LSU and MF processing of ASTER data: **a)** interpreted Fe-oxide–altered pixels overlain on bedrock geology map of the Microwave ridge area; **b)** interpreted Fe-oxide–altered pixels overlain on band 1 ASTER data; **c)** results overlain on RTP total-field aeromagnetic data; **d)** results overlain on first vertical-derivative (1VD) aeromagnetic data.

chlorite±calcite and Fe-oxide alteration. One of these zones corresponds to a region mapped as porphyritic granodiorite. It is speculated that the other two areas may similarly represent porphyritic granodiorite.

The three MINFILE occurrences on Microwave ridge include Cu-(Ag-Au) mineralization within the Telkwa Formation. The Stock (MINFILE 093L 085) and Table (MINFILE 093L 084) occurrences, on the southern slope of the ridge, lack a strong spectral response in their immediate vicinity despite good bedrock exposure. They occur along one of a series of northwest-trending minor faults. The northwesterly extension of the closest mapped fault corresponds with a clustered zone of possible iron-oxide and ferric iron-bearing minerals, flanked by Al-OH–bearing minerals, as indicated by ASTER processing. It is possible that the alteration is zoned away from a potential causative intrusion. The International (MINFILE 093L 086) occurrence, in contrast, is adjacent to one of the interpreted alteration zones and therefore may be proximal to a causative intrusion.

Acknowledgments

This manuscript benefited greatly from a thorough review by A. Fonseca. Excellent assistance for the field component of this investigation was provided by G. Lesage. Discussions with T. Richards provided valuable insight into the geology of the Skeena arch.

References

Angen, J.J., Nelson, J.L., Rahimi, M. and Hart, C.J.R. (2017): Mapping in the Tatsi and Zymo ridge areas of west-central British Columbia: implications for the origin and history of the Skeena Arch; *in* Geological Fieldwork 2016, BC Ministry of Energy, Mines and Petroleum Resources, BC Geological Survey, Paper 2017-1, p. 35–48.

Asadi Haroni, H. and Lavafan, A. (2007): Integrated analysis of ASTER and Landsat ETM data to map exploration targeting in the Muteh gold-mining area, Iran; *in* 5th International Symposium on Spatial Data Quality, XXXVI-2/C43, no. 5, Actas, June 13-15, 2007, Enschede, Netherlands, URL <http://www.isprs.org/proceedings/XXXVI/2-C43/Poster session/ASADI.pdf> [October 2017].

Azizi, H., Tarverdi, M.A. and Akbarpour, A. (2010): Extraction of hydrothermal alterations from ASTER SWIR data from east Zanjan, northern Iran; Advances in Space Research, v. 46, p. 99–109. doi:10.1016/j.asr.2010.03.014

BC Geological Survey (2017): MINFILE BC mineral deposits database; BC Ministry of Energy, Mines and Petroleum Resources, BC Geological Survey, URL <http://minfile.ca> [November 2017].

Beiranvand Pour, A. and Hashim, M. (2014): ASTER, ALI and Hyperion sensors data for lithological mapping and ore minerals exploration; Springer plus 2014, 19 p. doi:10.1186/2193-1801-3-130. URL: <http://www.springerplus.com/content/3/1/130> [October 2017].

Bierwirth, P.N. (2002): Evaluation of Aster satellite data for geological applications; consultancy report to Geoscience Australia, 50 p.

Boardman, J. W., Kruse, F. A. and Green, R. O. (1995): Mapping target signatures via partial unmixing of AVIRIS data; *in* Summaries of the Fifth JPL Airborne Earth Science Workshop, January 23-26, 1995, Pasadena, California, JPL Publication 95-1, v. 1, p. 23–26.

Clark, R.N., Swayze, G.A., Gallagher, A., King, T.V.V. and Calvin, W.M. (1993): The U.S. Geological Survey, Digital Spectral Library: Version 1: 0.2 to 3.0 microns; United States Geological Survey, Open File Report 9-592, 1340 p.

Colpron, M. and Nelson, J.L. (2011): A digital atlas of terranes for the northern Cordillera; accessed online from the Yukon Geological Survey, URL <http://www.geology.gov.yk.ca> [November, 2017].

Commonwealth Scientific and Industrial Research Organisation (2017): Mineral discovery and exploration; Commonwealth Scientific and Industrial Research Organisation website, URL <https://www.csiro.au/en/Research/Mining-manufacturing/Mineral-discovery-and-exploration> [November 2017].

Crowley, J. K., Brickey, W.D. and Rowan, C.L. (1989): Airborne imaging spectrometer data of the Ruby Mountains, Montana: mineral discrimination using relative absorption band-depth images; Remote Sensing of Environment, v. 29, p. 121–134.

Cui, Y., Miller, D., Nixon, G. and Nelson, J. (2015): British Columbia digital geology; BC Ministry of Energy, Mines and Petroleum Resources, BC Geological Survey, Open File 2015-2.

Desjardins, P., MacIntyre, D.G., Hunt, J., Lyons, L. and Pattenden, S. (1990): Geology of the Thautil River map area (93L/6); *in* Geological Fieldwork 1989, BC Ministry of Energy, Mines and Petroleum Resources, BC Geological Survey, Paper 1993-1, p. 91–99.

Evenchick, C.A., Poulton, T.P. and McNicoll, V.J. (2010): Nature and significance of the diachronous contact between the Hazelton and Bowser Lake groups (Jurassic), north-central British Columbia; Bulletin of Canadian Petroleum Geology, v. 58, p. 235–267.

Gagnon, J.F., Barresi, T., Waldron, J.F., Nelson, J.L., Poulton, T.P. and Cordey, F. (2012): Stratigraphy of the Upper Hazelton Group and the Jurassic evolution of the Stikine terrane, British Columbia; Canadian Journal of Earth Sciences, v. 49, p. 1027–1052.

Hewson, R.D., Cudahy, T.J. and Huntington, J.F. (2001). Geological and alteration mapping at Mt. Fitton, South Australia, using ASTER satellite-borne data; IEEE Transactions in Geoscience and Remote Sensing, p. 724–726.

Husdal, J. (1999): ERDAS Practical exercises website; University of Leicester, Leicester, United Kingdom, URL <https://erdas.wordpress.com/> [November 2017].

Jet Propulsion Laboratory (2017): Advanced Spaceborne Thermal Emission and Reflection Radiometer (ASTER); online information, URL<https://asterweb.jpl.nasa.gov/> [October 2017].

Kalinowski, A. and Oliver, S. (2004): ASTER Mineral Index Processing Manual; Remote Sensing Applications, Geoscience Australia, internal report, 39 p.

Lefebure, D.V. (1996): Cu+/-Ag quartz veins; *in* Selected British Columbia Mineral Deposit Profiles, Volume 2 – Metallic

Deposits; D.V. Lefebure and T. Hõy (ed.), BC Ministry of Employment and Investment, Open File 1996-13, p. 71–74.

Lefebure, D.V. and Church, B.N. (1996): Volcanic redbed Cu; *in* Selected British Columbia Mineral Deposit Profiles, Volume 2 – Metallic Deposits; D.V. Lefebure and T. Hõy (ed.), BC Ministry of Employment and Investment, Open File 1996-13, p. 5–7.

Lefebure, D.V. and Ray, G.E. (1998): Unconventional metal deposits in volcanic arcs; *in* Metallogeny of Volcanic Arcs, BC Geological Survey Branch, Short Course Notes, Open File 1998-8, Section I.

Mars, J.C. and Rowan L.C. (2006): Regional mapping of phyllic- and argillic-altered rocks in the Zagros magmatic arc, Iran, using Advanced Spaceborne Thermal Emission and Reflection Radiometer (ASTER) data and logical operator algorithms; Geosphere, v. 2, p. 161–186. doi:10.1130/GES00044.1

MacIntyre, D.G. (2006): Geology and mineral deposits of the Skeena Arch, west-central British Columbia: a Geoscience BC digital data compilation project; *in* Geological Fieldwork 2005, BC Ministry of Energy, Mines and Petroleum Resources, BC Geological Survey, Paper 2006-1, p. 303–312.

MacIntyre, D., Desjardins, P., Tercier, P. and Koo, J. (1989a): Geology of the Telkwa River Area, NTS 093L/11; BC Ministry of Energy, Mines and Petroleum Resources, BC Geological Survey, Open File 1989-16, 1:50 000 scale, URL <http://www.empr.gov.bc.ca/Mining/Geoscience/PublicationsCatalogue/OpenFiles/1989/Pages/1989-16.aspx> [November 2017].

MacIntyre, D.G., Desjardins, P. and Tercier, P. (1989b): Jurassic stratigraphic relationships in the Babine and Telkwa Ranges (93L/10, 11, 14, 15); *in* Geological Fieldwork 1989, BC Ministry of Energy, Mines and Petroleum Resources, BC Geological Survey, Paper 1989-1, p. 195–208.

Mather, P. (1999): Computer Processing of Remotely-Sensed Images: An Introduction; 2nd edition, John Wiley and Sons, 306 p.

Nelson, J. (2017): Composite pericratonic basement of west-central Stikinia and its influence on Jurassic magma conduits: examples from the Terrace-Ecstall and Anyox areas; *in* Geological Fieldwork 2016, BC Ministry of Energy, Mines and Petroleum Resources, BC Geological Survey, Paper 2017-1, p. 61–82.

Nelson, J.L., Barresi, T., Knight, E. and Boudreau, N. (2006): Geology and mineral potential of the Usk map area (103I/09) near Terrace, British Columbia; *in* Geological Fieldwork 2005, BC Ministry of Energy, Mines and Petroleum Resources, BC Geological Survey, Paper 2006-1, Report 2006-1, p. 117–134.

Nelson, J.L., Kyba, J., McKeown, M. and Angen, J.J. (2008): Terrace regional mapping project, Year 3: contributions to stratigraphic, structural and exploration concepts, Zymoetz River to Kitimat River, east-central British Columbia; *in* Geological Fieldwork 2007, BC Ministry of Energy, Mines and Petroleum Resources, BC Geological Survey, Paper 2008-1, p. 159–174.

Palomera, R.P.A. (2015): Spectral prospectivity mapping of Deseado Massif, Argentina: deciphering the geochemistry and mineralogy of a low to intermediate sulphidation epithermal system; University of Twente, Enschede, Netherlands, 220 p. doi:10.3990/1.9789036539067

Palsgrove, R.J. and Bustin, R.M. (1991): Stratigraphy, sedimentology and coal quality of the lower Skeena Group, Telkwa coalfield, central British Columbia (NTS 093L/11); BC Ministry of Energy, Mines and Petroleum Resources, BC Geological Survey, Paper 1991-2, 68 p.

Precision GeoSurveys Inc. (2016): Airborne Magnetic Survey, Search Project; Geoscience BC, Report 2016-02, 62 p.

Rajendran, S., Al-Khirbasha, S., Pracejusa, B., Nasira, S., Al-Abria, A.H., Kusky, T.M. and Ghulam, A. (2012). ASTER detection of chromite bearing mineralized zones in Semail Ophiolite Massifs of the northern Oman Mountains: exploration strategy; Ore Geology Reviews, v. 44, p. 121–135.

Ramachandran, B., Justice, C.O. and Abrams, M.J., editors (2010): Land Remote Sensing and Global Environment Change: NASA's Earth Observing System and the Science of ASTER and MODIS; Springer Verlag, New York, New York, 873 p. doi:10.1007/978-1-4419-6749-7

Robertson, W. F. (1917): Copper Queen; *in* Minister of Mines, Annual Report 1917, BC Ministry of Energy, Mines and Petroleum Resources, p. 119–120.

Rowan, L.C. and Mars, J.C. (2003). Lithologic mapping in the Mountain Pass, California area using Advanced Spaceborne Thermal Emission and Reflection Radiometer (ASTER) data; Remote Sensing of Environment, v. 84, no. 3, p. 350–366.

Rowan, L.C., Hook, S.J., Abrams, M.J. and Mars, J.C. (2003): Mapping hydrothermally altered rocks at Cuprite, Nevada, using the Advanced Spaceborne Thermal Emission and Reflection Radiometer (ASTER), a new satellite-imaging system; Economic Geology, v. 98, p. 1019–1027.

Sabins, F.F. (1997): Remote Sensing: Principles and Interpretation; 3rd edition, W.H. Freeman and Company, New York, New York, 494 p.

Shimabukuro, Y. E. and Smith, J. A. (1991): The least-squares mixing models to generate fraction images derived from remote sensing multispectral data; IEEE Transactions on Geoscience and Remote Sensing, v. 29, no. 1, p. 16–20.

Stanley, G. D. and McRoberts, C. A. (1993): A coral reef in the Telkwa Range, British Columbia: the earliest Jurassic example; Canadian Journal of Earth Sciences, v. 30, p. 819–831, URL <http://www.nrcresearchpress.com/doi/abs/10.1139/e93-068#.WfoZZHZxmM8> [November 2017].

Tipper, H.W. and Richards, T.A. (1976a): Jurassic stratigraphy and history of north-central British Columbia; Geological Survey of Canada, Bulletin 270, 73 p.

Tipper, H.W. and Richards, T.A. (1976b): Smithers map-area; Geological Survey of Canada, Open File 351, 1:253 440 scale.

Tseng, Y.H. (2000): Spectral unmixing for the classification of hyperspectral image; International Archives of Photogrammetry and Remote Sensing, v. XXXIII, Part B7.

United States Geological Survey (2017): Advanced Spaceborne Thermal Emission and Reflection Radiometer (ASTER); Global Visualization Viewer; United States Geological Survey, URL <https://glovis.usgs.gov/> [October 2017].

Van der Meer, F., Van der Werff, H., Van der Meijde, M., Van Ruitenbeek, F., Hecker, C. and de Jong, S. (2008): Object extraction and attribution from hydrospectral images; Chapter 15 *in* Advances in Photogrammetry, Remote Sensing and Spatial Information Sciences, Z. Li, J. Chen and E. Baltsavias (ed.), XXIst Congress of the International Society for

Photogrammetry and Remote Sensing, July 3–11, 2008, Beijing, China, congress book, p. 205–212.

Van Ruitenbeek, F.J.A., Cudahy, T.J., Van der Meer, F.D. and Hale M. (2012): Characterization of the hydrothermal systems associated with Archean VMS-mineralization at Panorama, Western Australia, using hyperspectral, geochemical and geothermometric data; Ore Geology Reviews, v. 45, p. 33–46.

Watts, D.R. and Harris, N.B.W. (2005): Mapping granite and gneiss in domes along the North Himalayan antiform with ASTER SWIR band ratios; Geological Society of America Bulletin, v. 117, no. 7/8, p. 879–886.